WATER RESOURCES RESEARCH, VOL. 36, NO. 6, PAGES 1583–1594, JUNE 2000

Estimation of erosion, deposition, and net volumetric change caused by the 1996 Skeiðarársandur jökulhlaup, Iceland, from synthetic aperture radar interferometry

Laurence C. Smith,[1] Douglas E. Alsdorf,[2] Francis J. Magilligan,[3] Basil Gomez,[4] Leal A. K. Mertes,[5] Norman D. Smith,[6] and James B. Garvin[7]

Abstract. Using repeat-pass satellite synthetic aperture radar interferometry, we develop a methodology to measure flood-induced erosion and deposition and apply it to a record 1996 glacier outburst flood (jökulhlaup) on Skeiðarársandur, Iceland. The procedures include (1) coregistration of backscatter intensity images to observe morphological differences; (2) mapping of interferometric phase correlation to identify preserved and modified surfaces; and (3) construction, correction, and differencing of pre-jökulhlaup and post-jökulhlaup topography. Procedures 1 and 2 are robust and should be widely applicable to other fluvial environments, while procedure 3 is complicated by uncertainties in phase measurement, baseline estimate, and atmospheric effects. After a correction procedure involving interpolation of digital elevation model elevation differences across low-correlation areas, we find ~4 m of elevation change are required to calculate volumes of erosion or deposition. This condition was satisfied for the 40 km^2 proglacial zone of Skeiðarársandur, where we estimate $+38 \times 10^6$ m^3 of net sediment deposition along the ice margin, -25×10^6 m^3 of net erosion in channels downstream, and a total net balance of $+13 \times 10^6$. These estimates are supported by field observations and survey data collected in 1997.

1. Introduction

Geomorphic impacts of large floods are normally evaluated at the cross-sectional or reach scale. Remotely sensed imagery from aircraft and satellites permit observation at broader scales but traditionally have been limited in their capability to directly measure flood-induced topographic change. Recently, synthetic aperture radar (SAR) interferometry has advanced our ability to obtain high-resolution measurements of topography and surface deformation on planetary surfaces. The method utilizes the phase shift between two coherent, slightly offset radar echoes from the same location on the ground. The magnitude of this phase shift is a function of surface elevation (and also any motion that has occurred), scaled by the physical distance or "baseline" between the two antenna positions. The required coherent radar echoes may be simultaneously acquired by a two-antennae system, such as the airborne TOPSAR and the forthcoming Shuttle Radar Topography Mission, or from single-antenna orbiting satellites (e.g., ERS-1, ERS-2, JERS-1, and Radarsat) that return to image the same location twice.

To date, applications of SAR to the study of fluvial processes have focused on the use of backscatter intensity images to map inundation [*Imhoff et al*., 1987; *Blyth and Biggin*, 1993; *Hess et al*., 1995; *Tholey et al*., 1997; *Oberstadler et al*., 1997], to stage [*Brakenridge et al*., 1994, 1998], or to estimate river discharge [*Smith et al*., 1995, 1996; *Smith*, 1997]. In this paper we present a first application of SAR interferometry to assess the distribution and volume of sediment erosion and deposition associated with a flood event. Specifically, we identify preserved and disturbed surfaces by their effect on interferometric phase correlation and estimate net topographic change by correcting and differencing interferometric topography before and after the flood. These results are validated with field surveys referenced to geodetic benchmarks, differential Global Positioning System (GPS), and field measurements of sediment erosion and deposition. Our case study is the 1996 glacier outburst flood (jökulhlaup) that occurred November 4–7 on the Skeiðarársandur, Iceland. Although jökulhlaups are a frequent occurrence at this locale [*Gudmundsson et al*., 1995], the 1996 event was conspicuous for its record magnitude and short duration [*Einarsson et al*., 1997]. Peak discharge has been estimated at 52,000 m^3 s^{-1} [*Jonsson et al*., 1998], with associated stream powers in the Gígjukvísl River ranging from 8×10^3 to 16×10^3 W m^{-2} [*Russell et al*., 1999]. The event affords a rare opportunity to study the effects of a high-energy flood pulse upon an unconfined braided outwash plain and may represent a useful analog for Pleistocene glacial-lake outburst floods along the margins of the Laurentide ice sheet [*Baker*, 1973; *Lord and Kehew*, 1987; *Kehew and Teller*, 1994]. Study of sediment dispersal patterns should also prove useful for evaluation of lithofacies models that have been developed in proglacial areas and subsequently applied to other environments, including humid alluvial fans [*Boothroyd and Nummedal*,

[1]Department of Geography, University of California, Los Angeles.
[2]Institute for Computational Earth System Science, University of California, Santa Barbara.
[3]Department of Geography, Dartmouth College, Hanover, New Hampshire.
[4]Geomorphology Laboratory, Indiana State University, Terre Haute.
[5]Department of Geography, University of California, Santa Barbara.
[6]Department of Geosciences, University of Nebraska at Lincoln.
[7]NASA Goddard Space Flight Center, Greenbelt, Maryland.

Paper number 1999WR900335.
0043-1397/00/1999WR900335$09.00

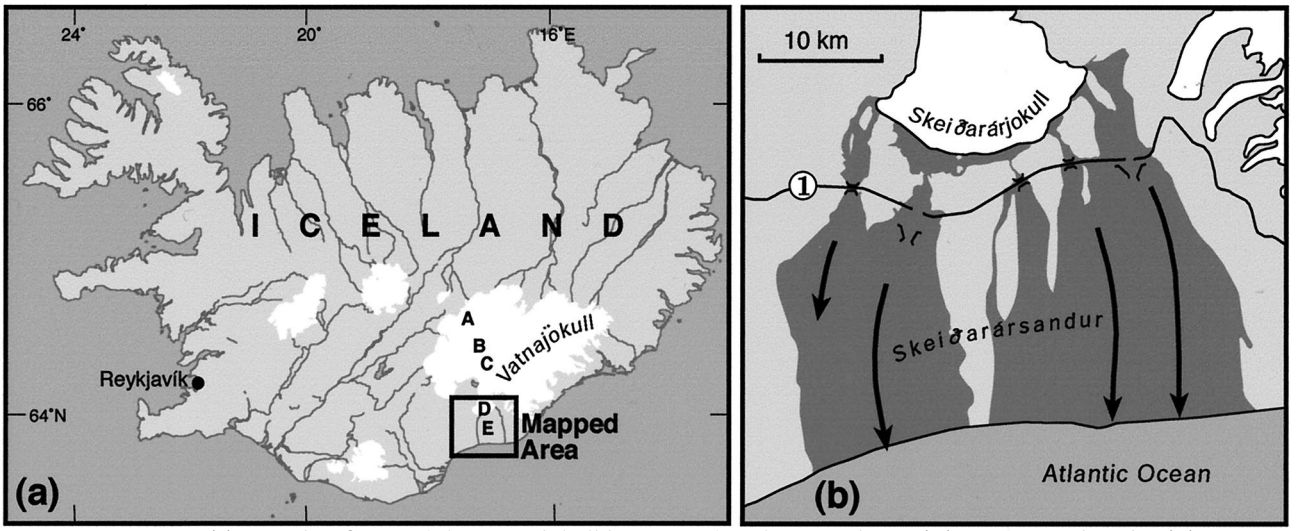

Figure 1. (a) Location figure of the Vatnajökull ice cap; Bárðarbunga volcano (A); 1996 eruption site (B); Grímsvötn subglacial caldera lake (C); the Skeiðarárjökull outlet glacier (D); and the Skeiðarársandur (outwash plain) (E). The square outlines the study area shown in more detail at right. (b) Maximum jökulhlaup extent on Skeiðarársandur at 15:40 on November 5, 1996. Inundation area is approximately 750 km^2. Figure 1b was adapted from digital base map provided by O. Sigurðsson, National Energy Authority, Iceland.

1978], petroleum reservoirs [*Maizels*, 1993a], and the Martian surface in the vicinity of the Viking 1 and Mars Pathfinder landing sites [*Rice and Edgett*, 1997]. A primary objective of this study was to assess the geomorphic impact of the 1996 jökulhlaup on Skeiðarársandur, particularly identification of any broad patterns of sediment erosion or dispersal. Therefore the vast area and large volumes of sediment involved led to our exploration of SAR interferometry as a complement to traditional field-based methods.

2. Study Area

Skeiðarársandur is the world's largest active braided outwash plain, covering an area of approximately 1250 km^2 (Figure 1). The sandur is characterized by a "type III" assemblage of lithofacies sequences, thought to have been deposited by a series of jökulhlaups [*Maizels*, 1991, 1993b]. These sequences are characteristically massive, coarsening upward, clast-supported pebbles and cobbles with basal gravels and capping of cross-bedded and horizontally bedded units [*Maizels*, 1993a; *Maizels*, 1997]. Jökulhlaups have historically occurred on the Skeiðarársandur every 1–7 years [*Gudmundsson et al*., 1995]. Although generally correlated with volcanic activity, eruptions are not required for jökulhlaups to occur. Meltwater from subglacial eruptions or geothermal heat flux drains into the subglacial Grímsvötn caldera lake, where increasing hydrostatic pressure eventually penetrates an ice dam found at the glacier bed [*Björnsson*, 1992]. The meltwater then flows subglacially for 50 km beneath Skeiðarárjökull before emerging onto Skeiðarársandur.

On September 10, 1996, a subglacial volcanic fissure eruption began beneath Vatnajökull ice cap between the Bárðabunga and Grímsvötn volcanoes (Figure 1a). The event continued for 13 days, forming a hyaloclastite ridge 6–7 km long and 200 m high under 500–750 m of ice [*Gudmundsson et al*., 1997]. The event caused significant changes in ice surface topography and flow velocities near the eruption site [*Gudmundsson et al*., 1997; *Alsdorf and Smith*, 1999]. For 5 weeks, meltwater flowed into the subglacial Grímsvötn caldera lake, increasing water storage to an estimated 3.6 km^3 [*Gudmundsson et al*., 1997]. On November 4, failure of the ice dam triggered the release of a jökulhlaup with the largest instantaneous discharge ever recorded on Skeiðarársandur. Flood flows first emerged in the Skeiðará River by 7:20 A.M. on November 5. Subsequent flow breakouts occurred progressively westward along the entire ice margin over the next 9 hours. By 15:40, flood waters were issuing along most of the entire 25 km length of the glacier terminus (Figure 1b). Hyperconcentrated flows are estimated to have issued from the glacier margin at velocities of up to 6 m s^{-1} [*Russell and Knudsen*, 1999]. The flood crest was attained in just 15 hours, at which time five primary channels were actively transporting water and sediment onto the sandur. With the exception of a narrow N-S strip running down the central sandur (Figure 1b), these flows coalesced to inundate about 750 km^2 or approximately 75% of the outwash plain [*Sigurðsson et al*., 1998].

In July 1997 we conducted field measurements to characterize effects of the 1996 jökulhlaup on Skeiðarársandur. Laser total station surveys were carried out along the Gígjukvísl, Skeiðará, and Nupsvötn outflow channels. Surveyed elevations were tied into geodetic benchmarks and located with differentially corrected GPS to assess the quality of our postflood interferometric digital elevation model (DEM). Along the Gígjukvísl and Skeiðará flow paths, eroded scarp heights and depths of fresh kettle holes were measured as proxies for erosion depth and minimum sediment deposition thickness, respectively. Differential GPS was also used to locate prominent ground features for georeferencing the SAR imagery.

3. Synthetic Aperture Radar (SAR) Data Processing and Model Validation

The ERS-1 and ERS-2 satellites acquired several pairs of radar images before and after the November 4–7 jökulhlaup

Table 1. Raw ERS-1 and ERS-2 SAR Data Processed in This Study

Dates	ERS-1 and ERS-2 Orbits	$\mathbf{B}_\perp$, m	$\mathbf{B}_\parallel$, m	h_a, m
March 27–28, 1996	24581-4908	15	13	647
October 21–22, 1996	27552-7879	−126	−87	76
October 23–24, 1996	27587-7914	77	36	124
January 1–2, 1997	28589-8916	−228	−70	34

Each pair consists of an ERS-1 image followed by an ERS-2 acquisition 1 day later. Perpendicular ($\mathbf{B}_\perp$) and parallel ($\mathbf{B}_\parallel$) baseline components are also shown. Ambiguity heights (h_a) indicate maximum topographic sensitivity for the October 21–22, 1996, and January 1–2, 1997, interferometric pairs. These pairs were processed further to obtain preflood and postflood topography of Skeiðarársandur.

with potential for interferometric analysis (Table 1). We processed the raw SAR signal data in three ways in order to (1) observe morphological changes (from backscatter intensity images); (2) detect surface disturbance (from interferometric phase correlation); and (3) quantify volumetric change (from elevation differences between preevent and postevent interferometric digital elevation models). The latter requires a correction procedure for baseline and atmospheric effects. Following a technical description of these procedures (section 3), interpretation and results are presented in section 4.

3.1. Radar Backscattering Intensity

The radar antennae on the ERS-1 and ERS-2 satellites measure both the amplitude and phase of the complex backscattered radar echo. For a given pixel element on the ground both are controlled by the orientation, distribution, and dielectric properties of its set of individual scatterers, with length scales of the order of the radar wavelength (5.6 cm for ERS). Thus the complex radar signal for each pixel is the coherent sum of echoes from its corresponding set of scattering elements [*Zebker et al.*, 1996]. Spatial averaging or "multilooking" of the raw single-look complex (SLC) signal data is used to increase the area over which this coherent sum is computed thus improving the local signal-to-noise ratio. Amplitude (a) and phase (ϕ) may be extracted from each complex number ($x + yi$) as $a = (x^2 + y^2)^{1/2}$ and $\phi = \arctan(y/x)$, respectively. Alternatively, each complex number may be expressed in polar form as $a(\cos\phi + i \sin\phi)$ or (a cis ϕ), permitting direct realization of a and ϕ.

Land-surface applications of radar imagery traditionally utilize only the amplitude component a, or "backscatter intensity," of the complex signal data. Backscatter intensity is sensitive to surface dielectric constant, roughness at the scale of the radar wavelength (5.6 cm for ERS), and local incidence angle. Temporal changes in these backscattering properties may be detected by constructing composite images that coregister backscatter intensity images of the same location acquired at different times. Such coregistration was implemented by calculating the local spatial correlation function for hundreds of regions throughout the images. The image offsets required to maximize the local correlation for each area were determined by cross correlation of the image intensities. These values were then used to calculate polynomial offset functions in range and azimuth across the entire image. Once the offset functions are known, two images may be coregistered to a subpixel precision of better than 0.1 pixel [*Wegmuller and Werner*, 1995]. Coregistered backscatter intensity images from March 27, 1996, and January 1, 1997, therefore yield a temporal composite image showing morphological changes on Skeiðarársandur (Plate 1).

3.2. Interferometric Phase Correlation

A normalized complex interferogram may be constructed from two coregistered SLC images by multiplying each complex number in the first SLC image by the complex conjugate

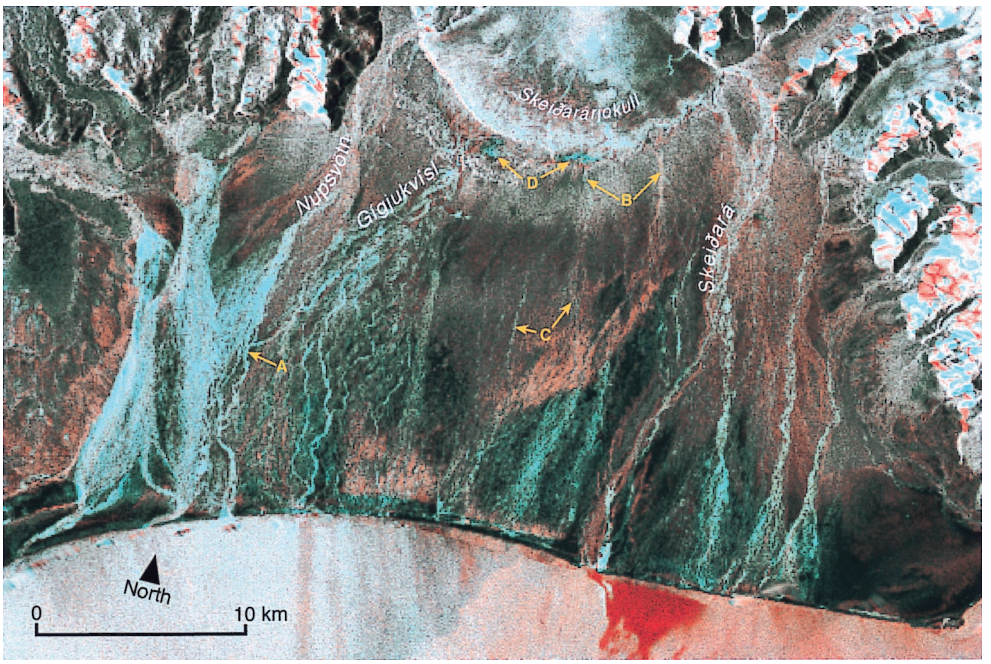

Plate 1. Coregistered radar backscattering intensity images, acquired March 27, 1996, (red) and January 1, 1997 (green). Blue tones indicate primary flow paths of the 1996 jökulhlaup. Also identified are a westward migration of the Gígjukvísl River (A), activation of overflow channels (B), incision of new channels in the central sandur (C), and the disappearance of two proglacial lakes (D).

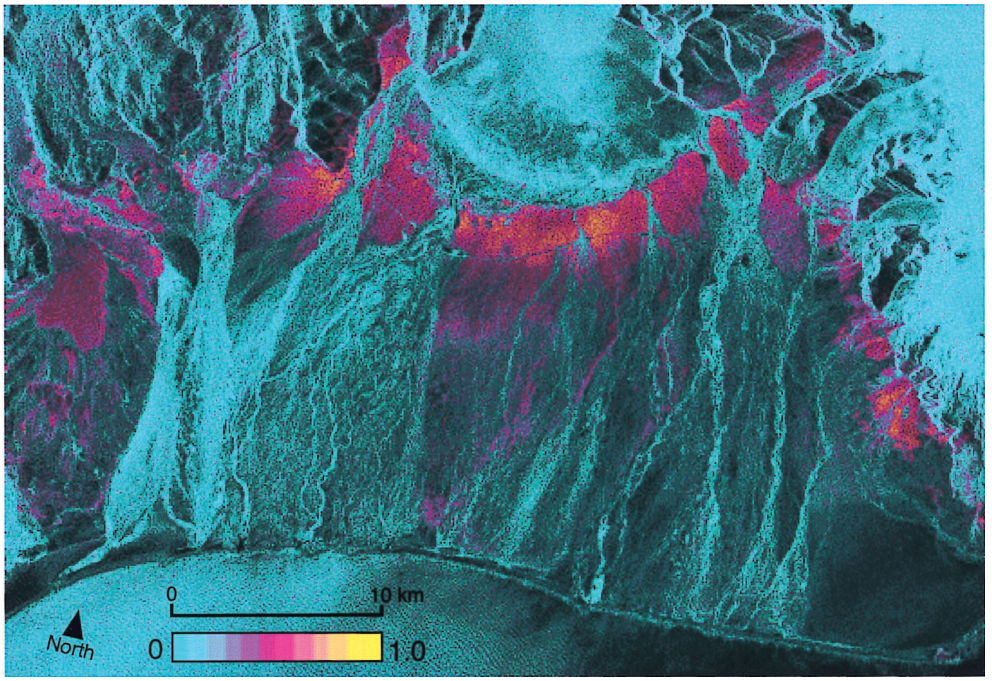

Plate 2. Interferometric phase correlation on the Skeiðarársandur between October 24, 1996, and January 2, 1997, overlain on the January 2 radar backscattering intensity image. Maximum correlation range is 0 to 1.0. High correlation (red and yellow hues) indicate surface preservation and therefore absence of significant erosion or deposition by the 1996 jökulhlaup. Isolation of the ice-proximal zone from the active glacier-sandur system is indicated by lenticular areas of high phase correlation. Moderate correlation in the central sandur indicates minor surface disturbance, despite partial inundation of this area.

of the corresponding complex number in the second SLC image and normalizing the result. Phase values of the resulting complex interferogram represent the interferometric phase difference between the two radar images. Amplitude values of the resulting normalized complex interferogram represent the amount of cross correlation between the complex values of the two SLC images. This total interferometric phase correlation c is derived from the two coregistered complex image values s_1 and s_2 as

$$c = \frac{|\langle s_1 s_2^* \rangle|}{\sqrt{\langle s_1 s_1^* \rangle \langle s_2 s_2^* \rangle}} \tag{1}$$

where asterisks denote complex conjugation and angular brackets denote statistical expectation, realized by spatial averaging within a rectangular filter and taking the absolute value of the numerator constrains correlation values to lie between 0 and 1.

Two coherent radar echoes will be correlated with each other if each has experienced the same or nearly the same interaction with a scatterer or set of scatterers. For orbital repeat-pass interferometry with nearly parallel tracks, three major factors will contribute to a loss of correlation between echoes: (1) thermal noise of the antennae (c_{thermal}), (2) a significant difference in viewing geometry that changes the relative locations of scattering centers and/or the amount of volume scattering (c_{spatial}), and (3) "temporal decorrelation" (c_{temporal}) resulting from an change in the positions of individual scattering elements on the imaged surface (e.g., the growth of vegetation) [*Zebker and Villasenor*, 1992]. All three correlation components contribute to the total interferometric phase correlation c calculated from the SAR data above ($c = c_{\text{thermal}} c_{\text{spatial}} c_{\text{temporal}}$). Inspection of a theoretical expression for the temporal component c_{temporal} [*Zebker and Villasenor*, 1992]

$$c_{\text{temporal}} = \exp\left\{ -\frac{1}{2}\left(\frac{4\pi}{\lambda}\right)^2 (\sigma_y^2 \sin^2\theta + \sigma_z^2 \cos^2\theta) \right\} \tag{2}$$

where λ is the radar wavelength and θ the incidence angle shows that for sensor viewing angles $\theta < 45°$ a greater sensitivity is expected for vertical changes (z) than for horizontal changes (y). Therefore surfaces with significant surface scattering will decorrelate less quickly than surfaces with significant volume scattering. The nominal incidence angle of the ERS-1 and ERS-2 satellites is 23°. This provides a favorable condition for measurement of phase correlation over moist gravel surfaces, where surface scattering dominates the returned radar echo.

Plate 2 shows the interferometric phase correlation c on Skeiðarársandur between October 24, 1996, and January 2, 1997. This image permits identification of areas that were disturbed or bypassed by the jökulhlaup. From (2) the temporal component c_{temporal} will rapidly decrease if the positions of microscattering elements on an imaged surface are disrupted over time, causing temporal decorrelation. Sediment resurfacing through erosion or deposition replaces a first set of surface scattering elements with a completely new set, which will generate a pattern of radar echoes that are incoherent with the first. This is the case even if the sediments composing the new surface have similar properties (i.e., grain-size distribution, dielectric constant, and slope) to the original surface. Temporal decorrelation in ERS SAR data has recently been used to permit unambiguous mapping of open water surfaces, regard-

less of clouds, darkness, wind, or turbulence [*Smith and Alsdorf*, 1998]. Because open water surfaces are constantly in motion at the scale of the radar wavelength, the aggregate phase return on a first acquisition date will be radically different from the phase return from a second acquisition, resulting in low values of phase correlation. Similarly, if flood deposition or scour creates a new scattering surface on a floodplain, phase correlation between an image acquired before the flood and an image acquired after the flood will be extremely low. While other phenomena can cause temporal decorrelation (e.g., vegetation growth, changing soil moisture, snowfall, etc.), areas that do yield high phase correlation can safely be assumed to indicate lack of any significant erosion or deposition.

3.3. Interferometric Digital Elevation Models and Topographic Change Images

By further processing a normalized complex interferogram, topographic height maps may be derived from SAR interferometry [*Zebker and Goldstein*, 1986; *Goldstein et al*., 1988; *Gabriel and Goldstein*, 1988; *Evans et al*., 1992]. The method is based on the principle that the difference in phase between two coherent radar echoes of a point on the imaged surface is a function of the elevation at that point and the baseline (physical distance between the antennae). If present, surface displacements also contribute to the phase shift and must be separated from the topographic component. Precision of the elevation measurement, or meters of topographic relief per 2π cycle of the phase difference, improves nonlinearly with the perpendicular component of the baseline. This quantity is variously referred to as the "height of ambiguity" or "altitude of ambiguity" [*Massonnet and Rabaute*, 1993] and is somewhat analogous to the contour interval of a topographic map. Heights of ambiguity (h_a) for the SAR image pairs examined in this study range from 34 m to 647 m and are presented along with perpendicular and parallel baseline components in Table 1.

To derive pre-jökulhlaup and post-jökulhlaup topography for Skeiðarársandur, the four pairs of tandem ERS-1 and ERS-2 images listed in Table 1 were processed using the gamma SAR processor and interferometry software [*Wegmuller and Werner*, 1997]. Processing began with the raw signal data and included estimation of the Doppler centroid, range compression, autofocusing, azimuth compression, and 1×5 resolution-cell averaging in the range and azimuth directions. Steps to construct DEMs included complex SAR image coregistration (described in section 3.1), interferogram generation, phase unwrapping, precise baseline estimation, computation of topographic heights, and resampling to universal transverse Mercatur coordinates with a 20 m pixel spacing. Inspection of ambiguity heights in Table 1 indicates good topographic sensitivity for the October 21–22 (h_a = 76 m) and January 1–2 (h_a = 34 m) image pairs but poor topographic sensitivity for the March 27–28 (h_a = 647 m) and October 23–24 (h_a = 124 m) image pairs. Therefore DEMs constructed for October 21–22 and January 1–2 were selected for comparison of pre-jökulhlaup and post-jökulhlaup topography.

Zebker et al. [1994a] show that errors in the estimates of interferometric phase and baseline can lead to significant errors in resulting DEMs. Baseline errors normally propagate systematically through the DEM and are effectively eliminated in our estimates of net topographic change, as will be described shortly. Phase errors are nonsystematic and represent the "pixel-to-pixel" accuracy of the derived DEM. Specifically,

$$\sigma_z = \frac{\lambda r}{4\pi B}[\sin\alpha - \cos\alpha \tan(\alpha - \theta)]\sigma_\phi, \qquad (3)$$

where σ_z and σ_ϕ are the deviations of height and phase, respectively, with radar wavelength λ, range r, incidence angle θ_ϕ, baseline separation B, and the angle of the baseline with respect to horizontal α [*Zebker et al*., 1994a]. Values of the phase standard deviation σ_ϕ are a function of the correlation c, with the magnitude of σ_z (the "pixel-to-pixel" uncertainty in the derived DEM) increasing with decreasing correlation. For the October 21–22, 1996, and January 1–2, 1997, pairs, correlation in the ice-proximal zone averaged 0.78 and 0.74, respectively. From (3) this yields average height errors of σ_z = 3.3 m for the preflood DEM and σ_z = 2.4 m for the postflood DEM. These values are reasonable, as the theoretical best minimum for σ_z with ERS data is 1.8 m [*Zebker et al*., 1994a]. Assuming an average σ_z value of 2.9 m suggests that at least 4.1 m of erosion or deposition should occur in order to detect volumetric change by subtracting interferometric DEMs.

In repeat-pass interferometry a third source of error results from temporal and spatial variations in atmospheric water vapor content. Slight radar propagation delays through a wet troposphere can lead to significant height errors (tens to hundreds of meters) in derived DEMs [*Goldstein*, 1995; *Rosen et al*., 1996; *Zebker et al*., 1997]. Such errors are nonsystematic with length scales of the order of kilometers (corresponding to the scale of spatial variations in water vapor content). Because the magnitude of propagation delay is independent of wavelength, errors from these atmospheric effects cannot be corrected with dual-frequency measurements [*Zebker et al*., 1997].

Systematic and nonsystematic errors from baseline and atmospheric effects, respectively, confound direct subtraction of independently constructed pre-jökulhlaup and post-jökulhlaup DEMs for topographic change. Therefore a correction procedure was developed to mitigate such errors. The correction is based upon the principle that regions that display high values of interferometric correlation c across the time of the flood are topographically stable, that is, have experienced no erosion or deposition and therefore should have the same elevation values. This correction was implemented in four steps: (1) The January 1–2 DEM was subtracted from the October 21–22 DEM. The resultant "elevation difference image" may contain height errors due to baseline and atmospheric uncertainties, as well as actual topographic change from flood erosion and deposition. (2) A new elevation difference image is created by masking areas of the first image that display low October–January correlation (see Plate 2). Topographic stability is assumed for the remaining areas of high correlation, permitting attribution of all elevation differences in these areas to systematic (i.e., baseline uncertainty) and/or nonsystematic (i.e., atmospheric effects) errors from either input DEM. (3) Elevation difference values in the masked (low correlation) areas are calculated by two-dimensional linear interpolation from adjacent high-correlation areas. This new, interpolated elevation difference image represents a model of the error field resulting from both baseline and atmospheric effects (Figure 2).

However, owing to the nonsystematic, kilometer-scale errors associated with atmospheric effects, confidence in this model is good for short interpolation gaps (i.e., smaller than the scale of tropospheric water vapor phenomena) but is poor across large interpolation gaps. Thus this correction procedure is considered valid across narrow fluvial channels with adjacent high-correlation areas such as found in the ice-proximal sandur but

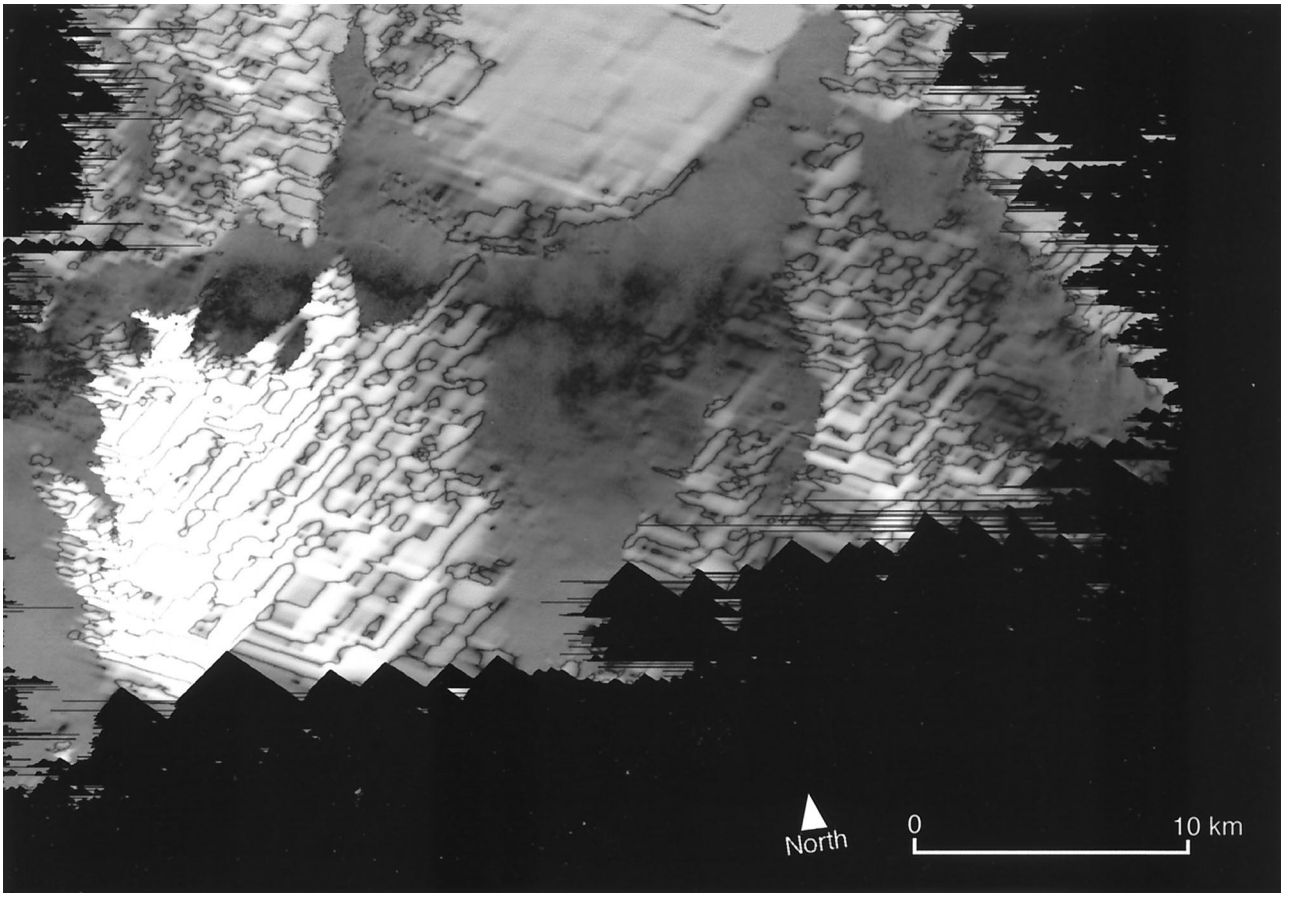

Figure 2. Modeled error field of Skeiðarársandur used to mitigate atmospheric and baseline effects between pre-jökulhlaup and post-jökulhlaup digital elevation maps (DEMs). Interpolation artifacts occur across expansive areas of low phase correlation, including glacier ice (top, center) and expansive flood inundation (bright tones to the left and right sides of Skeiðarársandur).

is considered unreliable across areas of expansive flood inundation on the central and distal sandur. (4) The modeled error field is subtracted from the original elevation difference image to yield a final image of net topographic change (Plate 3). Summation of this image over defined geographic areas yields net topographic budgets (volumetric change) for different parts of ice-proximal Skeiðarársandur (Table 2).

3.4. Model Validation

Ground-surface elevations obtained from laser total station surveys, referenced to nearby benchmarks, and spot estimates of "erosion depth" or "depositional thickness" from fresh scarp heights and kettle depths were used to test the accuracy of the postflood DEM and the topographic change map, respectively. Extraordinary sediment deposition between the ice margin and moraine complex was evidenced by massive, poorly sorted jökulhlaup deposits including matrix-supported outsized clasts, many in imbricated positions. Minimum thickness estimates for these deposits were collected by measuring the depths of 41 fresh kettle holes. Depths ranged from 1.5 m to 11.8 m. The kettle holes were formed by the melting of transported icebergs that were partially or completely buried by sediment deposition. Examination of stratification and sedimentary structures in the walls of freshly exposed kettle holes indicated that the surrounding deposits were strongly affected by flow-interference effects created by stationary icebergs. Where favorable exposures permitted, these effects could be observed to extend from the sandur surface to the base of the kettle. We thus infer that kettle depth is an approximate estimator of minimum deposition thickness and that scouring into the pre-jökulhlaup substrate was generally minimal.

Agreement between field-surveyed elevations and corresponding elevations from the postflood DEM is strongly linear (Figure 3). Assuming the field-surveyed elevations to be "correct," differences between field and interferometric elevation values are attributed to the uncertainties discussed earlier.

It is less straightforward to compare field observations of "erosion" or "deposition" with corresponding values in the topographic change image, because the field data are based upon stratigraphic interpretations tied into postflood elevation surveys and not the height difference between field surveys taken before and after the jökulhlaup. Therefore, while kettle depths and incised scarp heights may be reasonable indicators of minimum deposit thickness or incision depth, respectively, they may or may not reflect an increase or decrease in net elevation. For example, 10 m of initial scour in early flood stages followed by 10 m of waning-flow deposition will restore the surface its original elevation, resulting in a field observation of +10 m but a value of 0 m in the topographic change image. The 10 m of initial scour followed by 4 m of sediment deposition should yield a topographic change value of −6 m

and a field observation of +4 m. Such ambiguity can not be resolved using interferometry or any other topographic measurement based solely on surface elevations. Despite this uncertainty, field measurements of kettle depth and scarp height are in general agreement with interferometric estimates of net topographic change (Figure 4). All field observations of incision and most field observations of deposition correspond with negative and positive values in the topographic change image, respectively. Discrepancies between these two data sets may be due to errors in the topographic change image, the occurrence of both erosion and deposition at the same location, or the fact that kettle depths are only a minimum estimate of deposition.

4. Results

Merging of pre-jökulhlaup and post-jökulhlaup radar backscattering intensity images into a single temporal composite permits ready identification of maximum flood extent (Figure 5). Also revealed in this composite are alterations to the braided channel network, incision of new channels in the central sandur, activation of ephemeral overflow channels, and the disappearance of two small proglacial lakes. The Gígjukvísl River experienced significant channel widening and a westward migration of its primary flow path. While some areas of high radar backscattering were found to correspond to fields of stranded ice blocks [*Müschen et al*., 1997], field observations showed that ice distribution was not uniform across the sandur. High radar backscattering in backscatter intensity images is instead interpreted as an increased wetness of fluvial sediments [*Smith et al*., 1996] or the icing of receding flood waters.

High interferometric phase correlation is observed over lenticular portions of the ice-proximal zone (Plate 2), identifying large areas of the ice-proximal sandur that escaped resurfacing by the 1996 jökulhlaup. This clearly demonstrates that despite the large magnitude of this flood, much of the ice-proximal zone was isolated from its effects. Field visits to these high-correlation areas show them to be high-elevation relict depositional surfaces, with pervasive lichen and moss cover and evidence of extended weathering. Also of note are moderate correlation values found in the central sandur (Plate 2), indicating little erosion or deposition even though much of this area was inundated (Figure 1b and Plate 2). Field observations support this result: While minor inundation is indicated by intermittent slack water deposits, no evidence for significant erosion or deposition were found at sites on the central sandur.

Net topographic change for the ice-proximal zone is draped over the postevent DEM (for regional context) in Plate 3. As described in section 3.3, quality of the topographic change image is suspect over expansive areas of low phase correlation (e.g., over glacier ice and on the central and distal sandur). Therefore its construction was restricted to the area south of the glacier terminus and north of Highway 1. Note that the underlying DEM extends beyond these boundaries. Several considerations are critical to the correct interpretation of Plate 3: (1) The image represents net topographic change (i.e., the difference in elevation) between October 21–22, 1996, and January 1–2, 1997. This measure corresponds to the total aggradational thickness only where sediments are deposited directly onto an original surface. If scour occurs immediately prior to deposition, the height differential will be reduced by the depth of scour. This is advantageous for estimating net volumetric changes in topography but may cause the thickness of a particular sedimentary sequence to be underestimated if initial scour has occurred. (2) Values of the topographic change image are based on elevation change only and do not

Table 2. Volumes of Total Erosion, Deposition, and Net Change for (1) the Proglacial Area South of the Glacier Terminus and North of its Terminal Moraine; (2) the Area South of the Moraine and North of Highway 1; (3) Only the Breakout Channels Flowing Through the Moraine Complex; and (4) the Entire Ice-Proximal Zone of Skeiðarársandur (areas 1 and 2).

		Estimate 1		Estimate 2		Estimate 3	
	Area, km^2	Depth, m	Volume, $\times 10^6$ m^3	Depth, m	Volume, $\times 10^6$ m^3	Depth, m	Volume, $\times 10^6$ m^3
			North of Moraine				
Erosion	5.9	−4.9	−29.0	−6.0	−35.3	−6.4	−37.4
Deposition	7.9	+6.2	+49.3	+9.2	+72.9	+12.2	+96.5
Net	13.8	+1.5	+20.3	+2.7	+37.6	+4.3	+59.1
			South of Moraine				
Erosion	15.4	−3.0	−45.8	−3.2	−49.3	−3.5	−53.5
Deposition	10.3	+2.3	+23.2	+2.4	+24.5	+2.4	+25.1
Net	25.8	−0.9	−22.5	−1.0	−24.8	−1.1	−28.3
			Breakout Channels				
Erosion	2.6	−3.6	−9.3	−4.1	−10.8	−5.6	−14.7
Deposition	1.6	+2.9	+4.6	+3.3	+5.3	+3.5	+5.6
Net	4.2	−1.1	−4.6	−1.3	−5.5	−2.1	−9.0
			Entire Proximal Zone				
Erosion	21.2	−3.5	−74.6	−4.0	−84.4	−4.3	−90.4
Deposition	18.2	+4.0	+72.4	+5.3	+97.2	+6.7	+121.2
Net	39.5	−0.06	−2.2	+0.3	+12.8	+0.8	+30.8

Equivalent depths are also shown. For each geographic area, budgets are calculated from the topographic change image as the summation of all negative values (erosion), all positive values (deposition), and all values (net). Estimates 1, 2, and 3 provide a conservative range of values by imposing limits on the topographic change image of ±10 m, ±20 m, and no limits, respectively. Field observations support estimate 2 as a best estimate of net volumetric change from the 1996 jökulhlaup.

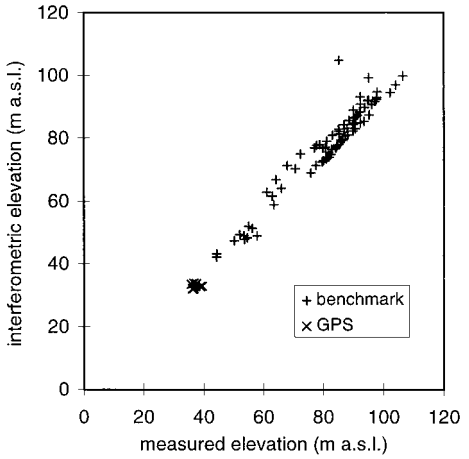

Figure 3. Comparison of post-jökulhlaup surface elevations (in meters above sea level (m asl)) on the Skeiðarársandur, as measured by field surveys and synthetic aperature radar interferometry ($R^2 = 0.97$, $\sigma = 3.6$, and confidence interval is 95%).

differentiate between different surface substrates. Ablation along the glacier terminus is therefore treated as topographic loss, while stranded ice blocks are treated as topographic gain. (3) Systematic height errors that may be present in either input DEM because of uncertainties in the estimates of satellite baseline have been removed as discussed. (4) Nonsystematic height errors from atmospheric effects are reduced where flow paths are narrow and flanked by high-correlation areas but may be problematic where flow paths are wide and/or not flanked by high-correlation areas.

Plate 3 reveals massive sediment deposition along the ice margin, with localized scour in breakout channels along the Skeiðará, Gígjukvísl, and Nupsvötn Rivers. Sediment deposition is particularly evident along the central and western terminus of Skeiðarárjökull, where it occurs in combination with a loss of ice to the north and erosion of the confining moraine complex to the south. Along the Gígjukvísl River, close-ups of pre-jökulhlaup and post-jökulhlaup DEMs, the topographic change image, and an aerial photograph taken during the flood reveals net channel widening, deepening, and the vertical accretion of a very large bar (Figure 5). These observations are in qualitative agreement with erosional and depositional patterns observed by the authors in the field, the first author from an aircraft, and by Icelandic scientists (O. Sigurðsson, personal communication, 1998).

Net topographic budgets for (1) the ice-marginal zone north of the moraine (between the glacier and its terminal moraine), (2) the area south (downstream) of the moraine, (3) in flow breakout channels, and (4) the entire ice-proximal zone (defined as the entire area between the glacier terminus and Highway 1) are presented in Table 2. Estimates of net erosion, deposition, and net volumetric change for each area are provided, assuming limits in the topographic change image of −10 to +10 m (estimate 1) and −20 to +20 m (estimate 2) and assuming no limits (estimate 3). Imposing these limits reduces the skew of net budget calculations introduced by extreme-valued pixels occasionally found in the topographic change image (plus/minus hundreds of meters) that are caused by local spatial errors in phase unwrapping or the modeled noise field. The three estimates thus provide a conservative range of estimates for net volumetric change of the ice-proximal zone of Skeiðarársandur. The three estimates share similar values of average erosion, average deposition, and net topographic change south of the moraine and within flow breakout channels. Greater discrepancy is found along the ice margin north of the moraine (average erosion is −4.9 to −6.4 m, average deposition is +6.2 to +12.2 m, and net change is +1.5 to +4.3 m). The variability, particularly among estimates of deposition, is likely due to (1) occurrence of more than +10 m of deposition (causing "estimate 1" to underestimate average deposition and therefore net topographic budget) and (2) the presence of only one stable topographic flank (the moraine) near the ice margin, reducing the quality of the modeled error (see section 3.3) near the glacier terminus. Glacier ice commonly yields low phase correlation and can also add a velocity component to the interferometric phase shift, introducing substantial error to the estimate of surface elevation. However, it is encouraging that despite these uncertainties, all three estimates indicate that significant deposition (~+6 to +12 m) occurred in front of the Skeiðarárjökull terminus, a result strongly supported by field observations (Figure 4).

In summary, a conservative range of net topographic budget estimates for the entire 40 km^2 ice-proximal zone suggests net volume gain (−2 to +31 × 10^6 m^3, Table 2). Note that these spatially integrated net estimates, in fact, result from substantial deposition along the ice margin (+50 to +96 × 10^6 m^3) offset by significant erosion downstream (−23 to −28 × 10^6 m^3). As Table 2 shows, further distributions exist between erosional and depositional processes within geographic areas (e.g., in the area south of the moraine complex, −46 to −53 × 10^6 m^3 of erosion is offset by +23 to 25 × 10^6 m^3 of deposition). Of the three estimates, estimate 2 (±20 m limit) probably yields the most realistic topographic budget, since there was no field evidence for >20 m of deposition, while kettle depths suggest that more than 10 m deposition did occur along parts of the ice margin. Therefore our best estimate of net

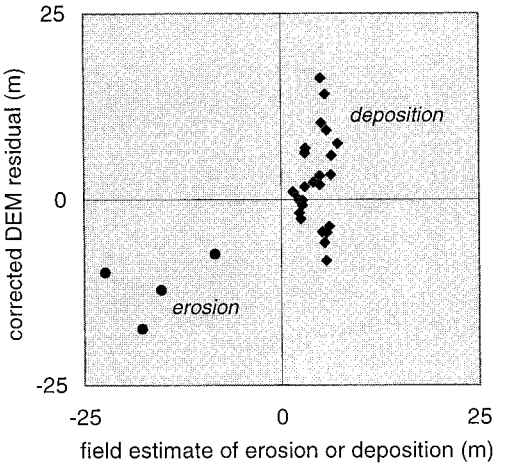

Figure 4. Comparison of stratigraphic measurements of erosion or deposition with corresponding values in the topographic change image. For each location the latter represents an interferometric estimate of net elevation change across the time of the jökulhlaup, while the field observation indicates the height of a freshly eroded scarp (circles, interpreted as erosion) or the depth of a kettle hole (diamonds, interpreted as minimum deposition) along the Gígjukvísl and Skeiðará flow paths ($R^2 = 0.43$, $\sigma = 5.9$, and confidence interval is 95%).

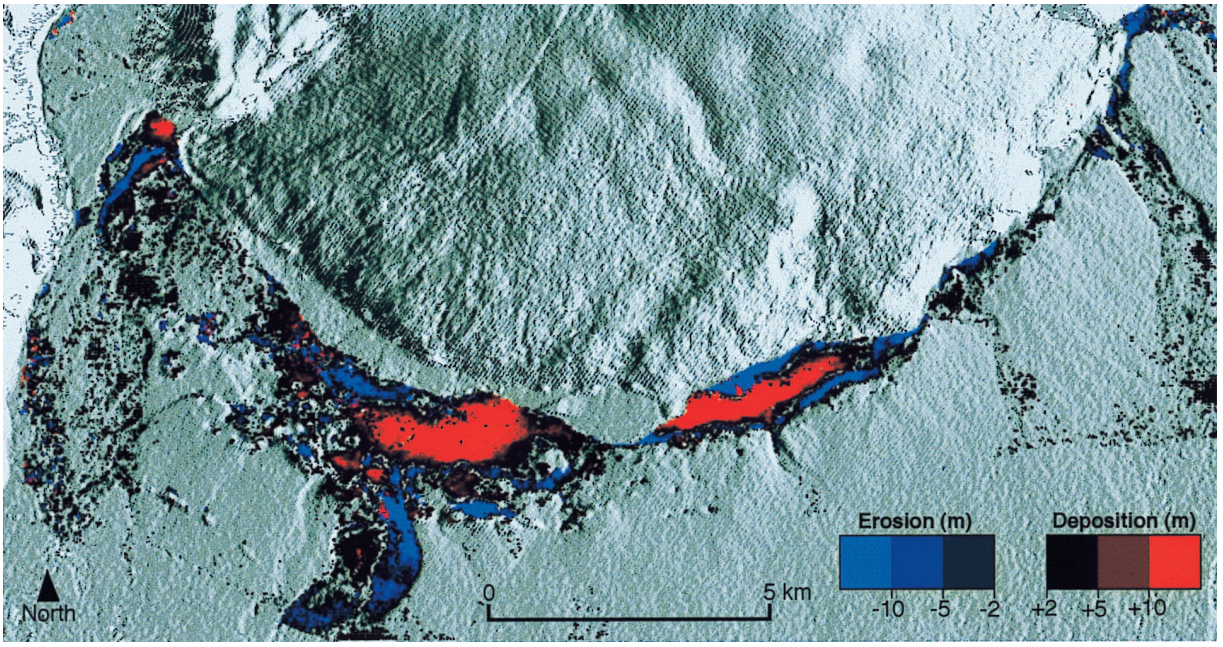

Plate 3. Net topographic change image for the ice-proximal Skeiðarársandur, overlain onto the postflood January 1–2, 1997, DEM. Red hues indicate net deposition; blues hues indicate net erosion. Thick deposition occurred along the ice terminus, with localized scour along the confining moraine/ice walls and in flow break-out channels. Severe channel incision and vertical accretion of a large bar on Gígjukvísl River occurred immediately downstream of its exit from the moraine complex. Close-ups of this area are shown in Figure 5.

topographic budget (estimate 2) is a positive volume gain of $+13 \times 10^6$ m^3 for the Skeiðarársandur ice-proximal zone, equivalent to +30 cm of deposition over this entire 40 km^2 area.

5. Discussion

We have utilized preevent and postevent SAR data in three ways to assess the geomorphic impact of the November 4–7, 1996, Skeiðarársandur jökulhlaup. Of the three procedures the use of interferometric correlation to detect disturbed surfaces and the differencing of interferometric DEMs to measure topographic change are new applications in fluvial geomorphology. Correlation mapping should be widely applicable to other fluvial environments, as the primary requirements for obtaining good correlation measurements are short physical and temporal baselines. The satellite vantage points should be close together and also follow closely in time before and after the jökulhlaup to reduce the likelihood of temporal decorrelation from other sources. However, DEM differencing is complicated by inherent errors in DEM construction, including baseline, phase estimate, and atmospheric uncertainties. Our results suggest that areas that experience ~4 m of net erosion or deposition can be clearly identified using tandem interferometric pairs with $h_a < 100$ m. This is in contrast to the centimeter-scale precision of differential interferometry studies of ice motion [e.g., *Kwok and Fahnestock*, 1996; *Joughin et al*., 1998] or crustal deformation [e.g., *Massonet et al*., 1993; *Zebker et al*., 1994b; *Peltzer and Rosen*, 1995], which is possible in situations where phase correlation is preserved everywhere across the time of motion. Fluvial erosion or deposition destroys the original scattering surface. This causes loss of correlation and therefore constrains interferometric analysis to the comparison of independently constructed interferometric DEMs which do not correlate across the time of the jökulhlaup. For this reason it is not currently possible to measure centimeter-scale elevation changes in fluvial environments with SAR interferometry. Such measurements should instead be sought with other active sensors such as airborne laser altimeters [e.g., *Krabill et al*., 1999; *Garvin et al*., 1998]. However, within the described constraints, topographic modification of large alluvial surfaces can be assessed by differencing preevent and postevent interferometric DEMs. Interferometry provides good spatial resolution (20 m in this study) and broad coverage (~100 km × 100 km). Global collections of ERS data archived since 1991 also permit establishment of preflood conditions nearly anywhere in the world.

Several insights into the erosional and depositional characteristics of the 1996 Skeiðarársandur jökulhlaup are provided by our observations: (1) Flows emerged from point sources and, with the exception of the ice-marginal zone and along preexisting flow paths, bypassed much of the ice-proximal sandur. This supports a conceptual model in which glacier retreat and lowering cause detachment of ice-marginal deposits from their source glacier. The mechanism for this detachment is channel entrenchment, which permits jökulhlaup flows to bypass much of the higher-elevation ice-proximal zone before widening into a braided channel configuration several kilometers downstream. A sequence of at least three sets of terraces mark the progression of such entrenchment on Skeiðarársandur [*Churski*, 1973]. (2) Enormous quantities of sediment were mobilized by the 1996 jökulhlaup with intense erosion and deposition near the ice margin and along river flow paths. The central Skeiðarársandur experienced little or no erosion or deposition, even where inundated. In the ice-proximal zone, erosion and deposition were widespread, with thick deposition near the glacier and erosion with some local-

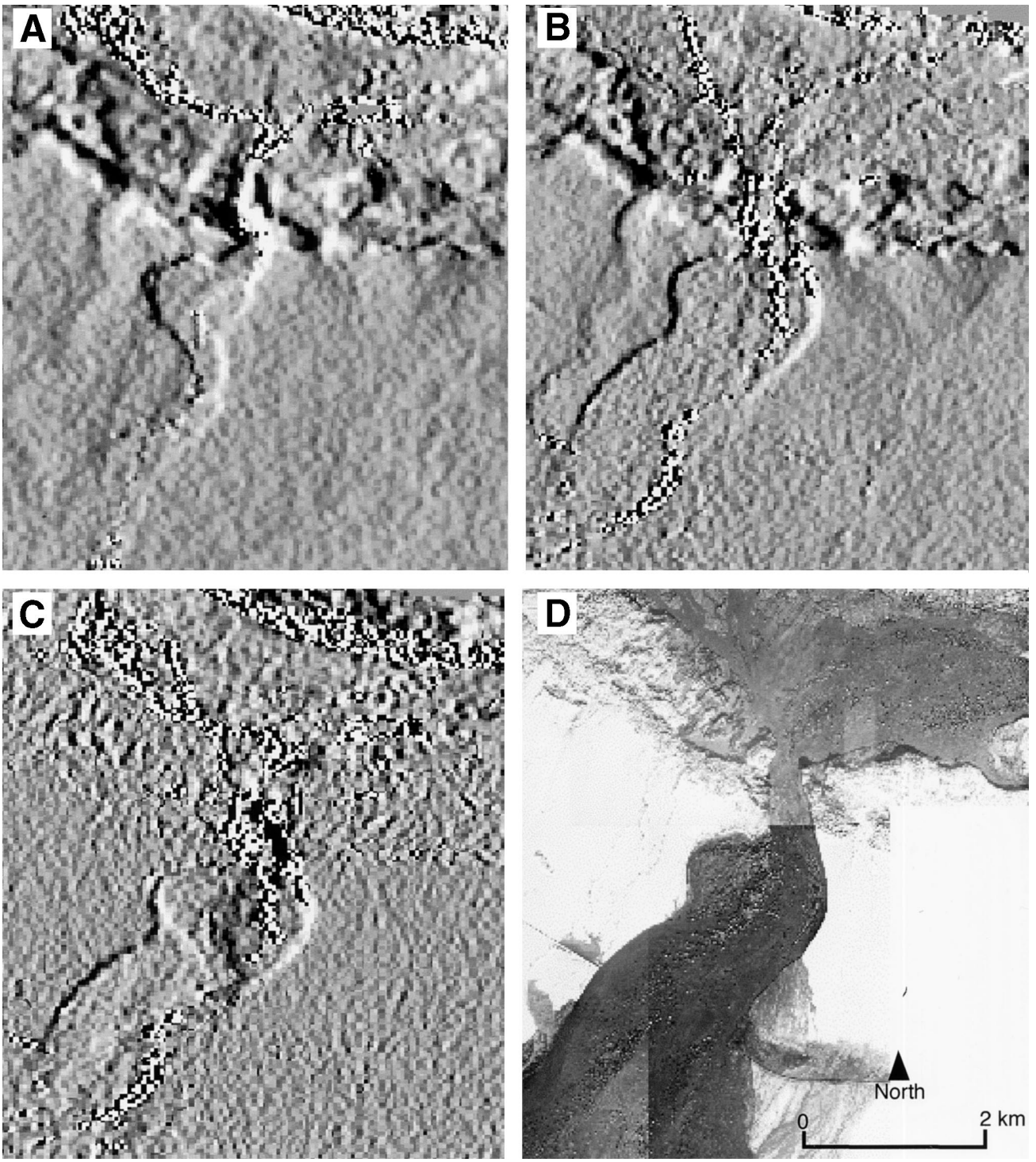

Figure 5. Topographic change along the upper course of Gígjukvísl: (a) pre-jökulhlaup interferometric DEM, (b) post-jökulhlaup interferometric DEM, (c) topographic change image, and (d) aerial photograph taken during the jökulhlaup (National Land Survey of Iceland photo 4993, November 11, 1996). In addition to channel widening and deepening the raised area in (C) reveals deposition of the large bar seen forming in the aerial photograph.

ized deposition downstream. Therefore much of the geomorphic work carried out by the 1996 jökulhlaup was expended by steepening the reach slope of its ice-proximal floodplain. *Maizels* [1993b] proposes a model for Icelandic sandur evolution in which episodic deposition of thick jökulhlaup sequences plays a primary role in construction of these landforms. Our interferometric and field observations of massive sediment deposition along the glacier margin provide support for this model. However, whether this large sediment pulse will be further distributed by future jökulhlaup events, from seasonal flows, or remain relatively intact remains unknown and will warrant investigation in future years.

6. Conclusions

Repeat-pass SAR interferometry is useful for assessing the impact of large floods on floodplain topography through disturbance mapping from loss of phase correlation and differencing interferometric digital elevation models (DEMs) to estimate volumetric change. A correction for baseline and/or atmospheric effects must be applied in the latter procedure.

Phase correlation mapping is robust and should be widely applicable to other fluvial environments. On the Skeiðarársandur, Iceland, high phase correlation across the time of the 1996 jökulhlaup reveals detachment of much of the ice-proximal sandur from the active glacier-outwash system, leading to a nonuniform response in sedimentation and erosion patterns across the floodplain. Vertical changes in elevation resulting from erosion and deposition of sediment and ice may be estimated by coregistering, correcting, and subtracting preflood and postflood interferometric DEMs. However, this approach is limited to very large or erosive events that experience ~4 m or more of elevation change. This condition was satisfied for the ice-proximal zone of the Skeiðarársandur, where we conservatively estimate net deposition of +20 to $+59 \times 10^6$ m^3 (+1.5 to +4.3 m) in the ice-marginal zone and net erosion of −23 to -28×10^6 m^3 (−0.9 to −1.1 m) downstream, with a net balance of −2 to $+31 \times 10^6$ m^3 (−0.06 to +0.8 m) for the entire 40 km^2 ice-proximal zone. Our best estimates, with vertical elevation changes constrained to lie within ±20 m, are $+38 \times 10^6$ m^3 (+2.7 m), -25×10^6 m^3 (−1.0 m), and 13×10^6 m^3 (+0.3 m), respectively.

Acknowledgments. This research was supported by a National Aeronautics and Space Administration, Land Surface Hydrology Program grant (NAG 5-7555) to L.C.S. and a National Science Foundation grant (SBR 9707648) to B.G. O. Sigurðsson (National Energy Authority, Iceland) provided valuable discussions and Icelandic base maps from which Figure 1b was adapted. We thank R. Bindschadler, M. Gudmundsson, and R. Williams for thoughtful and constructive reviews of an early version of this paper.

References

Alsdorf, D. E., and L. C. Smith, Interferometric SAR observations of ice topography and velocity changes related to the 1996 Gjalp subglacial eruption, Iceland, *Int. J. Remote Sens.*, *20*, 3031–3050, 1999.

Baker, V. R., Paleohydrology and sedimentology of Lake Missoula flooding in eastern Washington, *U.S. Geol. Surv. Spec. Pap.*, *144*, 79 pp., 1973.

Björnsson, H., Jökulhaups in Iceland: Prediction, characteristics, and simulation, *Ann. Glaciol.*, *16*, 95–106, 1992.

Blyth, K., and D. S. Biggin, Monitoring floodwater inundation with ERS-1 SAR, *Earth Obs. Quart.*, *42*, 6–8, 1993.

Boothroyd, J. C., and D. Nummedal, Proglacial braided outwash: A model for humid alluvial-fan deposits, *Can. Soc. Pet. Geol. Mem.*, *5*, 641–668, 1978.

Brakenridge, G. R., J. C. Knox, E. D. Paylor II, and F. J. Magilligan, Radar remote sensing aids study of the great flood of 1993, *Eos Trans. AGU*, *75*(45), 521, 526–527, 1994.

Brakenridge, G. R., B. T. Tracy, and J. C. Knox, Orbital SAR remote sensing of a river flood wave, *Int. J. Remote Sens.*, *19*, 1439–1445, 1998.

Churski, Z., Hydrographic features of the proglacial area of Skeiðarárjökull, *Geogr. Pol.*, *26*, 209–254, 1973.

Einarsson, P., B. Brandsdottir, M. T. Gudmundsson, H. Björnsson, F. Sigmundsson, and K. Grönvold, Center of Iceland hotspot experiences volcanic unrest, *Eos Trans. AGU*, *78*(35), 369, 374–375, 1997.

Evans, D. L., T. G. Farr, H. A. Zebker, and P. J. Mouginis-Mark, Radar interferometric studies of the Earth's topography, *Eos Trans. AGU*, *73*(52), 553, 557–558, 1992.

Gabriel, A. K., and R. M. Goldstein, Crossed orbit interferometry: Theory and experimental results from SIR-B, *Int. J. Remote Sens.*, *9*, 857–872, 1988.

Garvin, J. B., R. S. Williams, L. Smith, W. Krabill, and R. Swift, Pre- and post-jökulhlaup topography of the Skeiðarársandur, Iceland from laser altimetry, *Eos Trans. AGU*, *79*(17), Spring Meet. Suppl., S1, 1998.

Goldstein, R., Atmospheric limitations to repeat-track radar interferometry, *Geophys. Res. Lett.*, *22*(18), 2517–2520, 1995.

Goldstein, R. M., H. A. Zebker, and C. Werner, Satellite radar interferometry: Two-dimensional phase unwrapping, *Radio Sci.*, *23*(4), 713–720, 1988.

Gudmundsson, M. T., H. Björnsson, and F. Palsson, Changes in jökulhlaup sizes in Grímsvötn, Vatnajökull, Iceland, 1934–91, deduced from in-situ measurements of subglacial lake volume, *J. Glaciol.*, *41*(138), 263–272, 1995.

Gudmundsson, M. T., F. Sigmundsson, and H. Björnsson, Ice-volcano interaction of the 1996 Gjalp subglacial eruption, Vatnajökull, Iceland, *Nature*, *389*, 954–957, 1997.

Hess, L. L., J. M. Melack, S. Filoso, and Y. Wang, Delineation of inundated area and vegetation along the Amazon floodplain with the SIR-C synthetic aperture radar, *IEEE Trans. Geosci. Remote Sens.*, *11*, 1313–1325, 1995.

Imhoff, M. L., C. Vermillion, M. H. Story, A. M. Choudhury, A. Gafoor, and F. Polcyn, Monsoon flood boundary delineation and damage assessment using space borne imaging radar and Landsat data, *Photogramm. Eng. Remote Sens.*, *53*(4), 405–413, 1987.

Jonsson, P., A. Snorrason, and S. Palsson, Discharge and sediment transport in the jökulhlaup on Skeiðarársandur in November, *Eos Trans. AGU*, *79*(17), Spring Meet. Suppl., S13, 1998.

Joughin, I., R. Kwok, and M. Fahnestock, Interferometric estimation of three-dimensional ice-flow using ascending and descending passes, *IEEE Trans. Geosci. Remote Sens.*, *36*, 25–37, 1998.

Kehew, A. E., and J. T. Teller, History of late glacial runoff along the southwestern margin of the Laurentide ice sheet, *Quat. Sci. Rev.*, *13*(9–10), 10,859–10,877, 1994.

Krabill, W., E. Frederick, S. Manizade, C. Martin, J. Sonntag, R. Swift, R. Thomas, W. Wright, and J. Yungel, Rapid thinning of parts of the southern Greenland Ice Sheet, *Science*, *283*, 1522–1524, 1999.

Kwok, R., and M. A. Fahnestock, Ice sheet motion and topography from radar interferometry, *IEEE Trans. Geosci. Remote Sens.*, *34*, 189–200, 1996.

Lord, M. L., and A. E. Kehew, Sedimentology and paleohydrology of glacial-lake outburst deposits in southeastern Saskatchewan and northwestern North Dakota, *Geol. Soc. Am. Bull.*, *99*, 663–673, 1987.

Maizels, J. K., The origin and evolution of Holocene sandur deposits in areas of jökulhlaup drainage, Iceland, in *Environmental Change in Iceland: Past and Present*, edited by J. K. Maizels and C. Caseldine, pp. 267–302, Kluwer Acad., Norwell, Mass., 1991.

Maizels, J. K., Quantitative regime modelling of fluvial depositional sequences: Application to Holocene stratigraphy of humid-glacial braid-plains (Icelandic sandurs), in *Characterization of Fluvial and Aeolian Reservoirs*, edited by C. P. North and D. J. Prosser, *Geol. Soc. Spec. Publ.*, *73*, 53–78, 1993a.

Maizels, J. K., Lithofacies variations within sandur deposits: The role of runoff regime, flow dynamics and sediment supply characteristics, *Sediment. Geol.*, *85*, 299–325, 1993b.

Maizels, J. K., Jökulhlaup deposits in proglacial areas, *Quat. Sci. Rev.*, *16*(7), 793–819, 1997.

Massonnet, D., and T. Rabaute, Radar interferometry: Limits and potential, *IEEE Trans. Geosci. Remote Sens.*, *31*, 455–464, 1993.

Massonnet, D., M. Rossi, C. Carmona, F. Adragna, G. Peltzer, K. Feigl, and T. Rabaute, The displacement field of the Landers earthquake mapped by radar interferometry, *Nature*, *364*, 138–142, 1993.

Müschen, B., C. Böhm, A. Roth, M. Schwabish, and A. Holz, Monitoring of subglacial volcanic eruption and glacial flood in southern Iceland using ERS-1/2 SAR data, in *Proceedings of the International Seminar on the Use and Applications of ERS in Latin America, Vina del Mar, Chile*, *Eur. Space Agency Spec. Publ.*, *ESA SP-405*, 263–271, 1997.

Oberstadler, R., H. Honsch, and D. Huth, Assessment of the mapping capabilities of ERS-1 SAR data for flood mapping: A case study in Germany, *Hydrol. Processes*, *11*, 1415–1425, 1997.

Peltzer, G., and P. Rosen, Surface displacement of the 17 May 1993 Eureka Valley, California, earthquake observed with SAR interferometry, *Science*, *268*, 1333–1336, 1995.

Rice, J. W., and K. S. Edgett, Catastrophic flood sediments in Chryse Basin, Mars, and Quincy Basin, Washington: Application of sandar facies model, *J. Geophys. Res*., *102*(E2), 4185–4200, 1997.

Rosen, P. A., S. Hensley, H. A. Zebker, and F. H. Webb, Surface deformation and coherence measurements of Kilauea Volcano, Hawaii, from SIR-C radar interferometry, *J. Geophys. Res*., *101*(E10), 23,109–23,125, 1996.

Russell, A. J., and O. Knudsen, Controls on the sedimentology of November 1996 jökulhlaup deposits, Skeiðarársandur, Iceland, in *Advances in Fluvial Sedimentology VI*, edited by N. D. Smith and J. Rogers, *Spec. Publ. Int. Assoc. Sedimentol*., *28*, 315–329, 1999.

Russell, A. J., O. Knudsen, J. K. Maizels, and P. M. Marren, Channel cross-sectional area changes and peak discharge calculations on the Gígjukvísl during the November 1996 jökulhlaup, Skeiðarársandur, Iceland, *Jökull*, in press, 1999.

Sigurðsson, O., S. Vikingsson, and I. Kaldal, Course of events of the Jökulhlaup on Skeiarrsandur in November 1996, *Eos Trans. AGU*, *79*(17), Spring Meet. Suppl., S13, 1998.

Smith, L. C., Satellite remote sensing of river inundation area, stage, and discharge: A review, *Hydrol. Processes*, *11*, 1427–1439, 1997.

Smith, L. C., and D. E. Alsdorf, A control on sediment and organic carbon delivery to the Arctic Ocean revealed with satellite SAR: Ob'River, Siberia, *Geology*, *26*(5), 395–398, 1998.

Smith, L. C., B. L. Isacks, R. R. Forster, A. L. Bloom, and I. Preuss, Estimation of discharge from braided glacial rivers using ERS-1 SAR: First results, *Water Resour. Res*., *31*(5), 1325–1329, 1995.

Smith, L. C., B. L. Isacks, A. L. Bloom, and A. B. Murray, Estimation of discharge from three braided rivers using synthetic aperture radar (SAR) satellite imagery: Potential application to ungaged basins, *Water Resour. Res*., *32*(7), 2021–2034, 1996.

Tholey, N., S. Clandillon, and P. DeFraipont, The contribution of spaceborne SAR and optical data in monitoring flood events: Examples in northern and southern France, *Hydrol. Processes*, *11*, 1409–1413, 1997.

Wegmuller, U., and C. L. Werner, SAR interferometric signatures of forest, *IEEE Trans. Geosci. Remote Sens*., *33*, 1153–1161, 1995.

Wegmuller, U., and C. L. Werner, Gamma SAR processor and interferometry software, in *Proceedings of the 3rd ERS Symposium*, *Eur. Space Agency Spec. Publ*., *ESA SP-414*, 1686–1692, 1997.

Zebker, H., and R. Goldstein, Topographic mapping from interferometric SAR observations, *J. Geophys. Res*., *91*(B5), 4993–4999, 1986.

Zebker, H. A., and J. Villasenor, Decorrelation in interferometric radar echoes, *IEEE Trans. Geosci. Remote Sens*., *30*, 950–959, 1992.

Zebker, H. A., C. L. Werner, P. A. Rosen, and S. Hensley, Accuracy of topographic maps derived from ERS-1 interferometric radar, *IEEE Trans. Geosci. Remote Sens*., *32*, 823–836, 1994a.

Zebker, H. A., P. A. Rosen, R. M. Goldstein, A. Gabriel, and C. L. Werner, On the derivation of coseismic displacement fields using differential radar interferometry: The Landers earthquake, *J. Geophys. Res*., *99*, 19,617–19,634, 1994b.

Zebker, H. A., P. Rosen, S. H. Hensley, and P. J. Mouginis-Mark, Analysis of active lava flows on Kilauea volcano, Hawaii, using SIR-C radar correlation measurements, *Geology*, *24*(6), 495–498, 1996.

Zebker, H. A., P. A. Rosen, and S. Hensley, Atmospheric effect in interferometric synthetic aperture radar surface deformation and topographic maps, *J. Geophys. Res*., *102*(B4), 7547–7563, 1997.

D. E. Alsdorf, Institute for Computational Earth System Science, University of California, Santa Barbara, Santa Barbara, CA 93106. (alsdorf@icess.ucsb.edu)

J. B. Garvin, NASA Goddard Space Flight Center, Greenbelt, MD 20771. (garvin@denali.gsfc.nasa.gov)

B. Gomez, Geomorphology Laboratory, Indiana State University, Terre Haute, IN 47809. (gegomez@scifac.indstate.edu)

F. J. Magilligan, Department of Geography, Dartmouth College, Hanover, NH 03755. (Francis.J.Magilligan@Dartmouth.edu)

A. K. Mertes, Department of Geography, University of California, Santa Barbara, CA 93106. (leal@pollux.ucsb.edu)

L. C. Smith, Department of Geography, University of California, Los Angeles, 1255 Bunche Hall, Box 951524, 405 Hilgard Avenue, Los Angeles, CA 90095. (lsmith@geog.ucla.edu)

N. D. Smith, Department of Geosciences, University of Nebraska at Lincoln, Lincoln, NE 68588. (nsmith@unl.edu)

(Received May 17, 1999; revised November 23, 1999;
accepted November 24, 1999.)